Journal of Organometallic Chemistry 903 (2019) 120984

Contents lists available at ScienceDirect

Journal of Organometallic Chemistry

journal homepage: www.elsevier.com/locate/jorganchem

# Binuclear half-sandwich ruthenium(II) Schiff base complexes: Synthesis, characterization, DFT study and catalytic activity for the reduction of nitroarenes

Raja Nandhini [a], Bellie Sundaram Krishnamoorthy [b], Galmari Venkatachalam [a, *]

[a] PG & Research Department of Chemistry, Government Arts College, Dharmapuri, 636 705, Tamilnadu, India
[b] PG & Research Department of Chemistry, Vivekanandha College of Arts and Science for Women, Tiruchengode, Salem, Tamilnadu, India

ARTICLE INFO

*Article history:*
Received 5 September 2019
Received in revised form
11 October 2019
Accepted 14 October 2019
Available online 18 October 2019

*Keywords:*
Binuclear ruthenium
Schiff base
Synthesis
Crystal structure
DFT
Reduction of nitroarene

ABSTRACT

The binuclear ruthenium(II) *p*-cymene complexes containing Schiff base ligands of general composition [(Ru(*p*-cymene)Cl)$_2$L$_{1-6}$] (**1-6**) have been synthesized. The complexes were characterized by analytical and spectral (FT–IR, UV–Vis & $^1$H NMR) methods. The molecular structure of the representative complex [(Ru(*p*-cymene)Cl)$_2$(L$_6$)] **(6)** was determined by single-crystal X-ray diffraction and density functional theory (DFT) calculations. Further, these half-sandwich ruthenium complexes are active catalysts for the mild hydrogenation of nitroarenes to aromatic anilines in the presence of $NaBH_4$ in ethanol. The most efficient catalyst **6**, was found be compatible with nitroarenes of various functional groups.



## 1. Introduction

The arene ruthenium complexes play an important role in organometallic chemistry. Synthesis of half-sandwich ruthenium(II) complexes received a considerable attention owing to their catalytic properties [1] and interesting anti-tumor activity [2]. The half-sandwich ruthenium units with three-legged, piano-stool fragments are easy to prepare and are air-stable, where the piano-stool legs can be variably connected with O, N donor ligands [3–12]. The majority of half-sandwich ruthenium complexes have been prepared directly *via* reaction between various organic donors and half-sandwich ruthenium dimer precursors. Schiff base compounds are important O, N-based ligands which are readily modifiable to allow fine tuning of steric and electronic properties of the metal center [13].

The $\eta^6$-arene-ruthenium(II) complexes represent an important class of compounds [14], well-known for promoting a great variety of catalytic reactions, such as C–H activation [15], nitrile hydration [16] or transfer hydrogenation processes [17]. Aromatic anilines are important intermediates and precursors in the preparation of dyes, agrochemicals, pharmaceuticals, and pigments [18,19]. The most commonly used method for the synthesis of aromatic anilines is the reduction of nitroarenes. Catalytic hydrogenation using heterogeneous or homogeneous transition-metal catalysts is a well-established technique and is often employed for the reduction of nitroarenes to aromatic anilines [20–26]. There are many reports on the hydrogenation reaction of nitroarenes using transition metal catalysts in the presence of a reducing agent such as hydrogen gas, sodium tetrahydroborate, hydrazine, and alcohol as the hydrogen source. However, the use of well-defined half-sandwich ruthenium complexes containing Schiff-base ligands as homogeneous catalysts for hydrogenation of nitroarenes has rarely been reported. In comparison with previously reported half-sandwich ruthenium systems, ruthenium catalysts containing bulky naphthalene groups may exhibit higher catalytic activity for nitroarene reduction. The promising efficiency of these catalysts may be partially attributed to the strong electron-donating ability of the nitrogen and oxygen donors from Schiff base ligands.

We, prepare new half-sandwich binuclear ruthenium complexes with Schiff base ligands and hope to exploit their chemistry in catalytic reduction of nitroarenes. Preliminary results indicate that these complexes can catalyze nitroarene reduction in the

* Corresponding author.
*E-mail address:* gvchem@gmail.com (G. Venkatachalam).

https://doi.org/10.1016/j.jorganchem.2019.120984
0022-328X/

presence of $NaBH_4$ in ethanol. The electronic effects on their catalytic behavior of nitroarene reduction are also discussed. Computational chemistry tools are being used routinely to get more insight about the structural preferences and bonding nature of the metal complexes. Density Functional Theory (DFT) calculations at BP86/TZVP level are performed on the complex **6,** as a model to elucidate the electronic as well as geometrical structural features and bonding nature of these complexes.

## 2. Result and discussion

The dark red half-sandwich binuclear ruthenium(II) complexes (**1-6**) were obtained by the reaction of $[Ru(p\text{-cymene})(\mu\text{-}Cl)Cl]_2$ with an equivalent of the Schiff-base ligands in the presence of $Et_3N$ in $CH_2Cl_2$ under stirring at room temperature for 4 h (Scheme 1). Ruthenium complexes were isolated as pure complexes by chromatography on silica gel using EtOAC as an eluent in yields of 60–80%. All complexes have been characterized by IR, UV–Vis, $^1H$ NMR and mass spectrometry. The half-sandwich ruthenium complexes are air and moisture stable, soluble in $CH_2Cl_2$, $CHCl_3$ and $CH_3CN$.

The IR spectra of the Schiff bases ($H_2L_1$–$H_2L_6$) showed strong bands around 1619–1612 $cm^{-1}$ region are assigned for –CH=N stretching frequency. The C=N stretching frequencies displayed by the ruthenium(II) Schiff base complexes are lower than that for the uncomplexed ligands. This lowering of the C=N stretching frequency observed at 1595–1604 $cm^{-1}$ for these ruthenium complexes is attributed to coordination of C=N bonding in the chelate ring to the metal center. The FT–IR spectra of complexes **1–6** are given in Figs. S1–S6 (see supporting information).

Electronic spectra of all the complexes were recorded in chloroform solution at room temperature showed three bands in the region 200–800 nm. The UV–vis spectra of complexes **1–6** are given in Figs. S7–S12 (see supporting information). The high intensity bands in the 240–270 nm region were assigned to $\pi-\pi^*$ transitions of the ligands. The bands in the region 340–350 nm have been designated as $n-\pi^*$ transition of the non-bonding electron present on the nitrogen of the azomethine group [27]. In all the complexes, the lowest energy band observed in the region 430–450 nm were attributed to the metal to ligand charge transfer (MLCT) transitions [28–30].

The $^1H$ NMR spectra of all the ligands and complexes were recorded in $CDCl_3$ to confirm the coordination mode of the Schiff base ligand to the ruthenium(II) ion. The presence of the azomethine proton (–CH=N) attached to the phenyl ring was confirmed by the singlet around 8.3–8.9 ppm. The $^1H$ NMR spectra of complexes **1–6** are given in Figs. S13–S18 (see supporting information)The aromatic protons of all these complexes are observed as multiplets around 6.8–7.9 ppm. In all the complexes, the aromatic hydrogen's of *p*-cymene protons appear in the region of $\delta$ 4.4–5.5 ppm. Additionally, the methyl group of the *p*-cymene comes as a singlet around the region of $\delta$ 2.22–2.35 ppm. The isopropyl methyl protons of the *p*–cymene appeared as two sets of doublets in the region of $\delta$ 1.12–1.29 ppm. The methylene ($CH_2$) proton bridging the two phenyl rings in the complexes **1** and **5** was observed around 3.81 and 3.5 as a singlet. Additionally methoxy protons are observed as singlet for complexes **3** and **4** at $\delta$ 3.5 and 3.84 ppm respectively. The electrospray ionization (ESI) mass spectra of **4** and **5**, obtained in positive mode, give peaks at $m/z = 1008$ and 1046 respectively. The loss of one chloride atom for half-sandwich complexes is quite common under ESI-MS conditions [31–33].

The molecular structure of complex **6** was confirmed by single crystal X-ray diffraction and DFT methods. The crystals were grown by slow diffusion of chloroform into a concentrated solution of the complexes in pentane solution. The crystallographic data for binuclear half-sandwich ruthenium complexes **6** is summarized in Table 1. The molecular structure of **6** is shown in Fig. 1. The crystal packing was solved with monoclinic C2/c space groups. Each ruthenium is coordinated by one chlorine, one nitrogen and one oxygen atom from the Schiff base ligand and one of the *p*–cymene rings. The complex adopt the three legged piano stool geometry with σ-bonded Cl, N and O atoms as three legs and the arene ring of the *p*-cymene group forming the seat.

The Ru–O distances (2.061(3) and 2.057(3) Å and Ru–N distances (2.082(3) and 2.087(3) Å are comparable to those of a half–sandwich ruthenium complex containing [N, O] anionic bidentate ligands [34–36]. The DFT (BP86/TZVP) computed Ru–O distance of 2.039 Å and Ru–N distance of 2.088 Å are very close to the values obtained from experimental XRD method. The DFT (BP86/TZVP) computed Ru–Cl distance [2.427 Å] also very close to the experimentally obtained value 2.4339(13) Å. The metrical parameters obtained from XRD and DFT (BP86/TZVP) methods are provide in Table 2.

In the solid state, the complex exists as a solvate with chloroform. There are four molecules present in the asymmetric unit. The Ru–O distances 2.038(3) Å and Ru–N distances 2.073(4) Å are comparable to those of a half–sandwich ruthenium complex

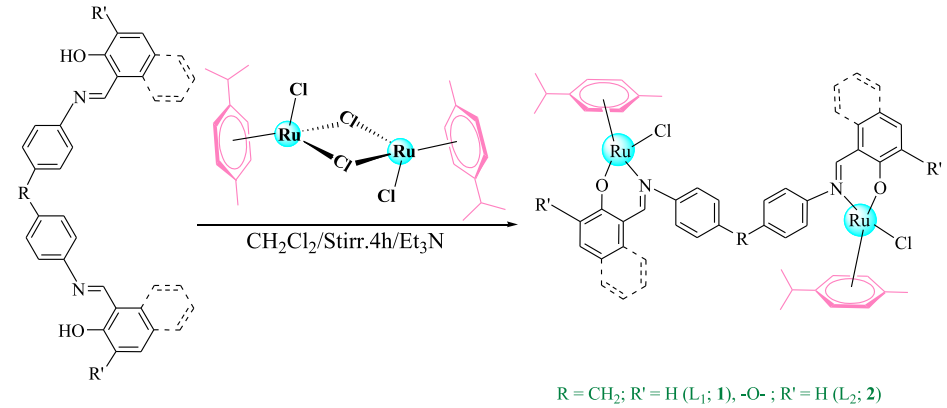


R = $CH_2$; R' = H ($H_2L_1$), -O- ; R' = H ($H_2L_2$)
R = $CH_2$; R' = $OCH_3$ ($H_2L_3$), -O- ; R' = $OCH_3$ ($H_2L_4$)
R = $CH_2$ ($H_2L_5$); -O- ($H_2L_6$)

R = $CH_2$; R' = H ($L_1$; **1**), -O- ; R' = H ($L_2$; **2**)
R = $CH_2$; R' = $OCH_3$ ($L_3$; **3**), -O- ; R' = $OCH_3$ ($L_4$; **4**);
R = $CH_2$ ($L_5$; **5**), -O- ($L_6$; **6**)

**Scheme 1.** Synthesis of Half-Sandwich Binuclear Ruthenium complexes (**1-6**).

**Table 1**
Selected crystal data and structure refinement summary of complex **6**.

| | 6 |
|---|---|
| Empirical formula | $C_{56}\ H_{51}\ N_2\ O_3\ Cl_5Ru_2$ |
| Formula weight | 1166 |
| Temperature | 298 |
| Wavelength/Å | 0.71073 Å |
| Crystal system | monoclinic |
| Space group | C2/c |
| a/Å | 22.4292 (11) Å |
| b/Å | 13.5674 (11) Å |
| c/Å | 19.3384 (13) Å |
| α/° | 90 |
| β/° | 107.202(5) |
| γ/° | 90 |
| Volume/Å$^3$ | 5621.6 (7) |
| Z | 4 |
| Density (calculated)/Mg/m$^3$ | 1.513 |
| Absorption coefficient/mm$^{-1}$ | 0.962 |
| F(000) | 2576 |
| Theta range for data collection/° | 1.777 to 29.110 |
| Reflections collected | 50476 |
| Independent reflections | 7556 [R(int) = 0.066] |
| Data/restraints/parameters | 7521/0/333 |
| Goodness-of-fit on F$^2$ | 1.314 |
| Final R indices [I > 2sigma(I)] | R1 = 0.062, w*R*2 = 0.2141 |
| R indices (all data) | R1 = 0.1284, w*R*2 = 0.1831 |

containing [N, O] anionic bidentate ligands [37–39]. The DFT (BP86/def2-TZVP) computed Ru—O distance of 2.039 Å and Ru—N distance of 2.088 Å are very close to the values obtained from experimental XRD method. The DFT (BP86/def2-TZVP) computed Ru—Cl distance 2.427 Å also very close to the experimentally obtained value 2.4339(13) Å. The metrical parameters obtained from XRD and DFT (BP86/def2-TZVP) methods are provided in Table 2 and the DFT optimized geometry is shown in Fig. 2.

The Ru—N, Ru—O and Ru—Cl bond lengths are close to the values of the similar type of geometry in the complexes and the geometrical features are important in deciding their structure-activity towards cancer cells [40]. In the solid state, the packing diagram of the compound **6** shows chain like array interconnected through the chlorine atoms and Schiff bases (Fig. S1) (See supporting information). Thus the presence of chlorine atom or halogen atom as leaving group in this type of molecules, ie., piano-stool ruthenium-arene complexes is already known, and which stabilizes the binuclear complex significantly in both solution and solid state.

In order to overcome the discrepancies experienced while solving the crystal structure, we have performed DFT calculations at BP86/def2-TZVP level, which helps to arrive the definite conclusion about the molecular structures of the complexes obtained. The charge on the metal atom is a crucial factor, which govern the catalytic activity of the complex. The DFT (BP86/def2-TZVP) computed charges on the two Ru atoms are +2 oxidation states. The information about the stability of the metal complexes are usually obtained by means computational methods. One of the best indicator is the energy gap $E_{LUMO\text{-}HOMO}$, as per Koopmanns' theorm. The significant $E_{LUMO\text{-}HOMO}$ gap value of 2.03 eV is in support with the stability of binuclear ruthenium complex **6** (Table 3**).** The DFT (BP86/def2-TZVP) computed frontier molecular orbitals (FMO) are highly useful in studying the stability of the bimetallic complex

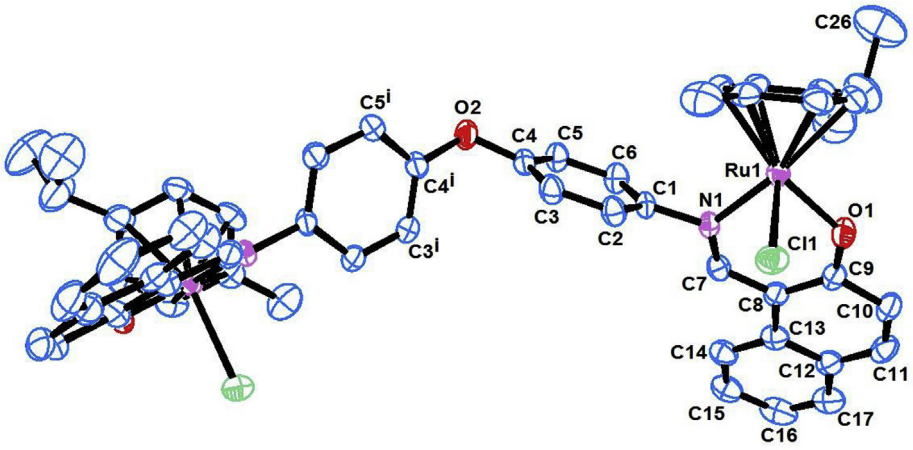


**Fig. 1.** ORTEP diagram of the complex [ $Ru_2Cl_2(\eta^6$–*p*–cymene$)_2Cl(L_6)$] (**6**).

**Table 2**
Selected bond lengths (Å) and Bond Angles (°) for Ruthenium Complex.

| Bond Length (Å) | | Bond Angle (°) | |
|---|---|---|---|
| $Ru_1$—$Cl_2$ | 2.4339(13) [2.427] | $N_5$—$Ru_1$—$O_4$ | 87.21(14) [86.80] |
| $Ru_1$—$N_5$ | 2.073(4) [2.088] | $N_5$—$Ru_1$—$Cl_2$ | 85.90(10) [85.08] |
| $Ru_1$—$O_4$ | 2.038(3) [2.039] | $O_4$—$Ru_1$—$Cl_2$ | 83.37(11) [83.20] |
| $Ru_1$—$C_{36}$ | 2.189(5) [2.197] | $N_5$—$Ru_1$—$C_{42}$ | 94.38(17) [95.23] |
| $Ru_1$—$C_{39}$ | 2.176(5) [2.191] | $O_4$—$Ru_1$—$C_{36}$ | 90.58(19) [89.78] |
| $C_{36}$—$C_{48}$ | 1.349(8) [1.438] | $O_4$—$Ru_1$—$C_{42}$ | 155.5(2) [155.72] |
| $C_{41}$—$C_{44}$ | 1.432(8) [1.486] | $N_5$—$Ru_1$—$C_{36}$ | 119.09(19) [120.46] |
| $C_{11}$—$O_3$ | 1.382(5) [1.398] | $O_4$—$Ru_1$—$C_{39}$ | 115.95(19) [115.97] |
| | | $N_5$—$Ru_1$—$C_{42}$ | 156.2(2) [156.40] |
| | | $C_{36}$—$Ru_1$—$C_{42}$ | 67.7(2) [68.32] |
| | | $C_{39}$—$Ru_1$—$Cl_2$ | 91.22(16) [91.29] |
| | | $C^{42}$—$Ru_1$—$Cl_2$ | 121.15(17) [121.08] |
| | | $C_{11}$—$O_3$—$C_{65}$ | 118; 42 [117.87] |

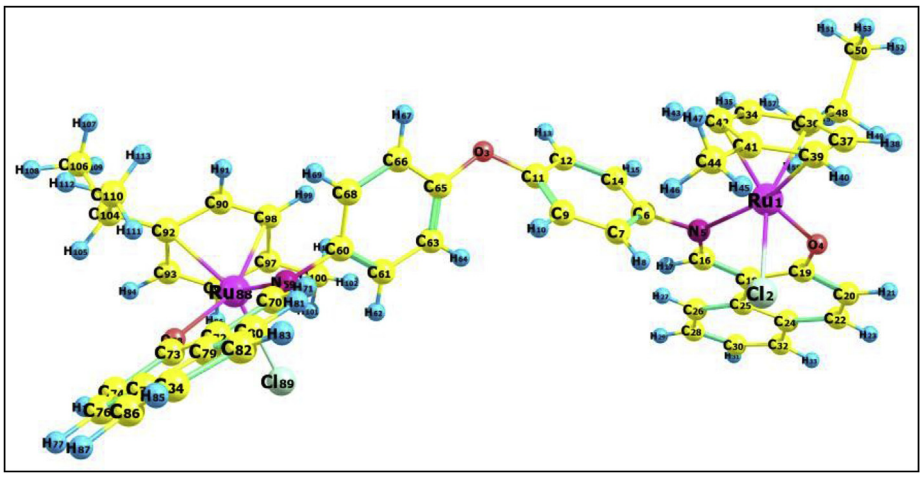


**Fig. 2.** The DFT (BFP86/def2-TZVP) optimized geometry of the complex **6**.

through the orbital energies and delocalization of electrons. The molecular orbital pictures of the FMOs (HOMO, LUMO, HOMO-1 and LUMO+1) obtained from DFT computation is presented in Fig. 3. From the HOMO picture of the complex, significant amount electron localization on the Ru atoms and Cl atoms whereas in the LUMO the no orbitals of the halogen atoms are involved. The bonding interactions between one of the Ru atom with Cl and arene ring is higher in HOMO, where as in HOMO-1 the interaction of second Ru atom with Cl and arene ring is higher. The involvement of the orbitals of O and N and the delocalization of electrons on the ring stabilizes the LUMO and LUMO+1orbitals. The DFT (BP86/def2-TZVP) computed reactivity descriptors like, Chemical potential(μ), Hardness (η), Softness(S), Electrophilicity (ω), Ionization potential (IP) and Electron Affinity (EA) values are provided in Table 3. The DFT computed hardness value is in line with the stability of complex **6,** and the electron affinity and electrophilicity values suggest the electrophilic nature of diruthenium-Schiff base complex.

The catalytic performance of half-sandwich binuclear ruthenium complexes **1–6** has been evaluated for reduction of nitroarenes with 1-chloro-4-nitrobenzene as a model substrate. As shown in Table 4, the binuclear half-sandwich ruthenium complex **6** was very active towards reduction of nitro compounds. The complex **6** was chosen as the optimal catalyst to screen various solvents (Table 4, entries 1–16). A high yield of 95% of the desired products was achieved in ethanol solvent. No desired products were detected in water due to the poor solubility of the catalyst (Table 4, entry 11). As expected, no reaction was observed in the control experiment performed without both base and the catalyst (Table 4, entry 14). From these studies, the optimal conditions for the reduction of nitroarenes were using **6** as catalyst (1 mol %) in the presence of four equivalents of $NaBH_4$ at room temperature.

With the optimal reaction condition in hand, we started to expand the scope and efficiency of this methodology. Many functionalized anilines were obtained in excellent yields (Table 5). As shown in Table 4, the catalyst **6** was found to be very active toward the reduction of various nitro compounds. Electron-withdrawing and electron-donating substituents on the aromatic ring were converted to the desired products in high yields. However, reduction of nitrotoluene generally takes a long time for an electron-donating group such as $-CH_3$ or $-OCH_3$ (Table 5, entries 8–10). Chemoselective reduction of the nitro group in the presence of other substituents such as −CHO, −COMe and −COOH was performed (Table 5, entries 3–5). Overall, the present nitroarene reduction protocol is simple to operate and gives the corresponding aniline in good to excellent yields.

A possible reaction mechanism for the reduction of nitroarenes is shown in Scheme 2. The proton signal at −10.18 ppm corresponds to a hydride, which indicates the presence of a Ru−H intermediate. Then, the reduction of the nitroarene may be proposed to occur via the outer-sphere mechanism (intermediate B), which gives the hydroxyl amine first and then the final aryl amine [41].

## 3. Conclusion

In summary, we have synthesized and characterized a series of novel half-sandwich binuclear ruthenium(II) complexes with binucleating Schiff-base ligands and examined their ability as catalysts in hydrogenation of nitroarenes using sodium tetrahydroborate as hydride source in ethanol solvent. The hydrogenation

**Table 3**
**DFT** (BFP86/def2-TZVP) computed reactivity descriptors like, Chemical potential. (μ), Hardness (η), Softness(S), Electrophilicity (ω), Ionization potential (IP) and Electron Affinity (EA) values (eV).

| Complex | 6 |
|---|---|
| HOMO | −4.4496 eV |
| LUMO | −2.4226 eV |
| $E_{LUMO\ -\ HOMO}$ | 2.0270 eV |
| Chemical potential $(\mu) = E_{LUMO+HOMO}/2$ | −3.4361 eV |
| Hardness $(\eta) = E_{LUMO\ -HOMO}/2$ | 1.0135 eV |
| Softness $(S) = 1/\eta$ | 0.9867 eV |
| Electrophilicity $(\omega) = \mu^2/2\eta$ | 5.8248 eV |
| Ionization potential (IP) (eV) | 4.4496 eV |
| Electron Affinity (EA) (eV) | 2.4226 eV |

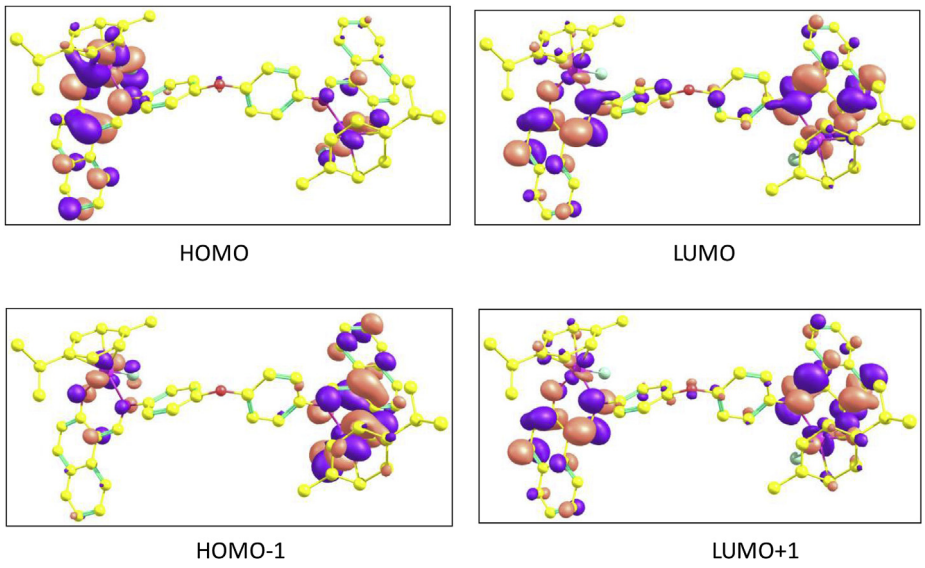


**Fig. 3.** The DFT (BFP86/def2-TZVP) computed frontier molecular orbitals (FMOs) of the complex **6** with iso surface value of 0.03.

**Table 4**
Screening of half-sandwich ruthenium complexes catalysts for nitroarene Reduction[a].

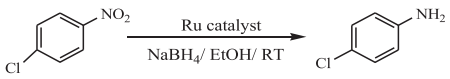


| Entry | Catalyst | Solvent | Time (h) | Yield (%)[b] |
|---|---|---|---|---|
| 1 | **1** | EtOH | 3 | 60 |
| 2 | **2** | EtOH | 3 | 73 |
| 3 | **3** | EtOH | 3 | 70 |
| 4 | **4** | EtOH | 3 | 75 |
| 5 | **5** | EtOH | 3 | 83 |
| 6 | **6** | EtOH | 3 | 95 |
| 7 | **6** | MeOH | 6 | 30 |
| 8 | **6** | DCM | 5 | 55 |
| 9 | **6** | Toluene | 8 | 28 |
| 10 | **6** | DMF | 10 | 48 |
| 11 | **6** | THF | 12 | 10 |
| 12 | **6** | MeCN | 10 | 42 |
| 13 | **6** | $H_2O$ | 24 | No Product |
| 14 | **-** | EtOH | 3 | No Product |
| 15 | **6** | EtOH | 3 | 92[c] |
| 16 | **6** | EtOH | 5 | 88[d] |

[a] Reaction conditions: 0.3 mmol 1-chloro-4-nitrobenzene, 1.2 mmol $NaBH_4$, Ru catalyst (3 mol%), solvent (2 mL), room temperature.
[b] Isolated yield.
[c] **6** (1 mol%)
[d] **6** (0.5 mol%).

reaction offers varied functional group compatibility and broad substrate scope and provides aromatic anilines in excellent yields The advantages of these homogeneous half-sandwich ruthenium catalyst systems include the case of catalyst synthesis and high catalytic activities toward nitroarene reduction in the presence of $NaBH_4$ in ethanol at room temperature. Moreover, a combination of spectroscopic studies and X-ray crystallographic and DFT (BP86/def2-TZVP) studies also confirmed the piano-stool geometry for the molecular structure of the half-sandwich binuclear ruthenium complexes. Molecular Orbital calculations and computation of reactivity descriptors also confirm the stability and electrophilic nature of these complexes.

## 4. Experimental methods

### 4.1. Materials and physical measurements

All the reagents used were chemically pure and of analytical grade. The solvents were freshly distilled before use. $RuCl_3 \cdot 3H_2O$ was purchased from Himedia Pvt. Ltd., and was used without further purification. α-Phellandrene, 2-hydroxy -1- naphthaldehyde, O-vanillin and 4,4′-diaminophenyl methane, 4,4′-diaminiphenyl ether were purchased from Sigma-Aldrich. The Schiff base ligands were prepared according to literature reports [42,43]. The starting materials $[(\eta^6\text{-}p\text{-cymene})_2Ru_2(Cl_2)_2]$, were prepared according to published methods [44]. The IR spectra of the complexes were recorded on an agilent resolution pro model in 4000−400 $cm^{-1}$ range. Electronic spectra of the complexes were recorded in $CHCl_3$ solution in a Cary 300 Bio UV−Vis Varian spectrophotometer in the range 800−200 nm. The $^1H$ NMR spectra were recorded in $CDCl_3$ with Bruker 300 MHz instrument using TMS as internal reference.

### 4.2. Synthesis of Half-sandwich binuclear ruthenium complexes (1–6)

A solution of the chloro bridged dimeric complex (0.06 g; 0.1 mmol), Schiff base ligands (0.040−0.0501 g; 0.1 mmol) and triethylamine in dichloromethane (30 mL) was added and mixture was stirred for 4 h at room temperature. A color change of the solution from dark red was observed. The solution was concentrated to 2 mL, and hexane was added to initiate precipitation of the complex. The red-brown powder was filtered and washed with hexane, and purified using column chromatography.

#### 4.2.1. *[(Ru(p-cymene)Cl)$_2$L$_1$]**(1)***

Red-brown solid. Yield: 70%. M.p. 180 °C. Anal. Calcd for $C_{47}H_{40}N_2Cl_2O_2Ru_2$: C, 60.25; H, 4.27; N, 2.99. Found: C, 59.02; H, 4.12; N, 2.59. FT–IR $cm^{-1}$): 1610 $\nu$(CH=N), 1325$\nu$(C−O). UV−Vis λmax (nm): 450,340, 270. $^1H$ NMR (300 MHz, $CDCl_3$): $\delta$(ppm) = 6.9−7.8 (m, Ar−H), 8.9 (s, HC=N), 3.8 (s, $CH_2$), 4.4 (d 1H, cymene Ar−H), 5.1 (d 1H, cymene Ar−H), 5.4 (d 1H, cymene Ar−H), 3.2 (m, 1H, CH of *p*–cymene), 2.3 (s,3H, $CH_3$ of *p*–cymene), 1.2 (dd,

**Table 5**
Screening of substrate for nitroarene reduction catalyzed by complex 6.[a].

| Entry | Substrate | Product | Yield (%)[b] |
|---|---|---|---|
| 1 | 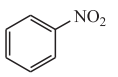 | 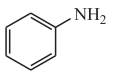 | 88 |
| 2 | 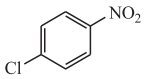 | 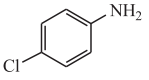 | 95 |
| 3 | 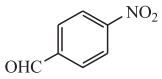 | 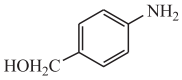 | 94 |
| 4 | 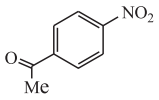 | 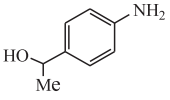 | 90 |
| 5 | 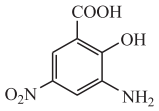 | 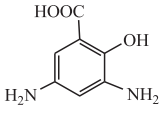 | 80 |
| 6 | 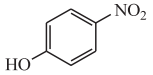 | 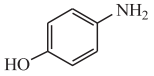 | 92 |
| 7 | 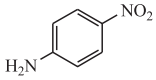 | 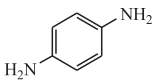 | 96 |
| 8 | 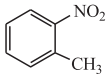 | 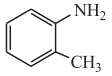 | 90 |
| 9 | 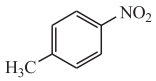 | 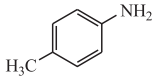 | 95 |
| 10 | 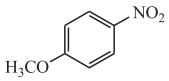 | 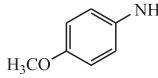 | 92 |
| 11 | 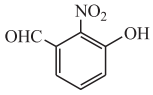 | 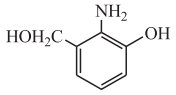 | 82 |

[a] Reaction conditions: 0.3 mmol nitroarene, 1.2 mmol $NaBH_4$, catalyst (1 mol%), solvent (2 mL), room temperature (3 h).
[b] Isolated yield.

6H, $2CH_3$ of *p*–cymene).

*4.2.2. [(Ru(p-cymene)Cl)$_2$L$_2$]**(2)***

Red-brown solid. Yield: 78%. M.p.200 °C. Anal. Calcd for $C_{46}H_{38}N_2Cl_2O_3Ru_2$: C, 58.8; H, 4.05; N, 2.98. Found: C, 58.02; H, 3.95; N, 2.86. FT–IR $cm^{-1}$): 1607 $\nu$(CH═N), 1328$\nu$(C–O). UV–Vis λmax (nm): 440, 330, 250.$^1$H NMR (300 MHz, $CDCl_3$): $\delta$(ppm) = 7.1–7.9 (m, Ar–H), 8.5 (s, HC═N), 4.4 (d 1H, cymene Ar–H), 5.1 (d 1H, cymene Ar–H), 5.3–5.5 (d 1H, cymene Ar–H), 3.2 (m, 1H, CH of *p*–cymene), 2.2 (s,3H, $CH_3$ of *p*–cymene), 1.12 (dd, 6H, $2CH_3$ of *p*–cymene).

*4.2.3. [(Ru(p-cymene)Cl)$_2$L$_3$]**(3)***

Red solid. Yield: 75%. M.p.230 °C. Anal. Calcd for $C_{49}H_{46}N_2Cl_2O_4Ru_2$: C, 58.44; H, 4.37; N, 2.80. Found: C, 58.39; H, 4.15; N, 2.76. FT–IR $cm^{-1}$): 1595$\nu$(CH═N), 1330$\nu$(C–O). UV–Vis λmax (nm): 450, 340, 270. $^1$H NMR (300 MHz, $CDCl_3$): $\delta$(ppm) = 6.9–7.9 (m, Ar–H), 8.3 (s, HC═N), 3.8 (s, $CH_2$), 3.5 (s, 3H, $OCH_3$), 4.4 (d 1H, cymene Ar–H), 5.1 (d 1H, cymene Ar–H), 5.5 (d 1H, cymene Ar–H), 2.3 (s,3H, $CH_3$ of *p*–cymene), 1.29 (dd, 6H, $2CH_3$ of *p*–cymene).

*4.2.4. [(Ru(p-cymene)Cl)$_2$L$_4$]**(4)***

Brown solid. Yield: 78%. M.p.190 °C. Anal. Calcd for $C_{48}H_{44}N_2Cl_2O_5Ru_2$: C, 57.14; H, 4.16; N, 2.8. Found: C, 57.06; H, 4.02; N, 2.72. FT–IR $cm^{-1}$): 1604 $\nu$(CH═N), 1330 $\nu$(C–O). UV–Vis λmax (nm): 450, 320, 270. $^1$H NMR (300 MHz, $CDCl_3$): $\delta$(ppm) = 6.8–7.8 (m, Ar–H), 8.4 (s, HC═N), 4.4 (d 1H, cymene Ar–H), 5.2 (d 1H, cymene Ar–H), 5.4 (d 1H, cymene Ar–H), 3.84 (s, 3H, $OCH_3$), 3.2 (m, 1H, CH of *p*–cymene), 2.3 (s,3H, $CH_3$ of *p*–cymene), 1.2 (dd, 6H, $2CH_3$ of *p*–cymene).

*4.2.5. [(Ru(p-cymene)Cl)$_2$L$_5$]**(5)***

Red–brown solid. Yield: 80%. M.p.210 °C. Anal. Calcd for $C_{55}H_{52}N_2Cl_2O_2Ru_2$: C, 63.09; H, 4.97; N, 2.67. Found: C, 62.80; H, 4.90; N, 2.50. FT–IR $cm^{-1}$): 1600 $\nu$(CH═N), 1340 $\nu$(C–O). UV–Vis λmax (nm): 460, 330, 270. $^1$H NMR (300 MHz, $CDCl_3$): $\delta$(ppm) = 6.8–7.9 (m, Ar–H), 8.6 (s, HC═N), 3.8 (s, $CH_2$), 5.2 (d 1H, cymene Ar–H), 3.1 (m, 1H, CH of *p*–cymene), 2.2 (s,3H, $CH_3$ of *p*–cymene), 1.21 (dd, 6H, $2CH_3$ of *p*–cymene).

*4.2.6. [(Ru(p-cymene)Cl)$_2$L$_6$]**(6)***

Red–brown solid. Yield: 78%. M.p.185 °C. Anal. Calcd for $C_{54}H_{50}N_2Cl_2O_3Ru_2$: C, 61.83; H, 4.77; N, 2.67. Found: C, 61.73; H, 4.65; N, 2.58. FT–IR $cm^{-1}$): 1601 $\nu$(CH═N), 1340 $\nu$(C–O). UV–Vis λmax (nm): 450, 320, 270. $^1$H NMR (300 MHz, $CDCl_3$): $\delta$(ppm) = 6.8–7.9 (m, Ar–H), 8.7 (s, HC═N),4.4 (d 1H, cymene Ar–H), 5.0 (d 1H, cymene Ar–H), 5.2 (d 1H, cymene Ar–H), 3.2 (m, 1H, CH of *p*–cymene), 1.29 (dd, 6H, $2CH_3$ of *p*–cymene).

*4.3. General procedure for the reduction of nitroarenes to anilines with half-sandwich*

*4.3.1. Binuclear ruthenium catalysts*

A half-sandwich binuclear ruthenium complex (1 mol%) was dissolved in EtOH (2.0 mL); then appropriate nitroarenes (0.3 mmol) and $NaBH_4$ (1.2 mmol) were added. The resulting mixture was stirred at room temperature in a closed vessel. After completion of the reaction (monitored by TLC), the crude reaction mixture was extracted with ether (3 × 2 mL). After the solvents were removed in vacuo from the combined organic extracts, the crude products were loaded directly onto a column of silica gel and purified by column chromatography using petroleum ether and ethyl acetate (1:3) to get the corresponding products.

*Aniline*. Yellow oil, yield: 88%. $^1$H NMR (500 MHz, $CDCl_3$): $\delta$ 7.32 (m, 2H), 6.94 (m, 1H), 6.48 (m, 2H), 3.6 (br, 2H).

*4-Chloroaniline*. Colorless solid, Yield: 95%. $^1$H NMR (300 MHz, $CDCl_3$): $\delta$ 7.1 (d, 2H), 6.62 (d, 2H), 3.62 (br, 2H).

*(4-Aminophenyl)methanol*. Pale yellow solid; yield: 94%. $^1$H NMR (300 MHz, $CDCl_3$): $\delta$ 7.12 (d, 2H), 6.69 (d, 2H), 4.4 (s, 2H), 3.4 (br, 2H).

*1-(4-Aminophenyl)ethanol*. Pale yellow solid; yield: 90%. $^1$H NMR (300 MHz, $CDCl_3$): $\delta$ 7.2 (d, 2H), 6.65 (d, 2H), 4.73 (m, 1H), 3.2 (br, 2H), 1.45 (d,3H).

*4-Aminophenol*. Brown solid; yield: 92%. $^1$H NMR (300 MHz, $CDCl_3$): $\delta$ 6.51 (t, 4H), 4.35 (s, $NH_2$).

*1,4-Phenylenediamine*. Red solid; yield: 96%. $^1$H NMR (300 MHz, $CDCl_3$): δ6.6 (s, 4H), 3.3 (br, 4H),

*2-Toluidine*. Yellow oil; yield: 90%.$^1$H NMR (300 MHz, $CDCl_3$): $\delta$ 7.2 (t, 2H), 6.8 (t, 1H), 6.6 (d, 1H), 4.3 (br, 2H), 2.28 (s, 3H).

*4-Toluidine*. Colorless solid; yield: 95%. $^1$H NMR (300 MHz, $CDCl_3$): $\delta$ 7.1 (d, 2H), 6.55 (d, 2H), 3.48 (br, 2H), 2.35 (s, 3H).

*p-Anisidine*. Orange solid; yield: 92%. $^1$H NMR (300 MHz, $CDCl_3$): $\delta$ 6.6 (d, 2H), 6.51 (d, 2H), 3.9 (s, 3H), 3.2 (br, 2H).

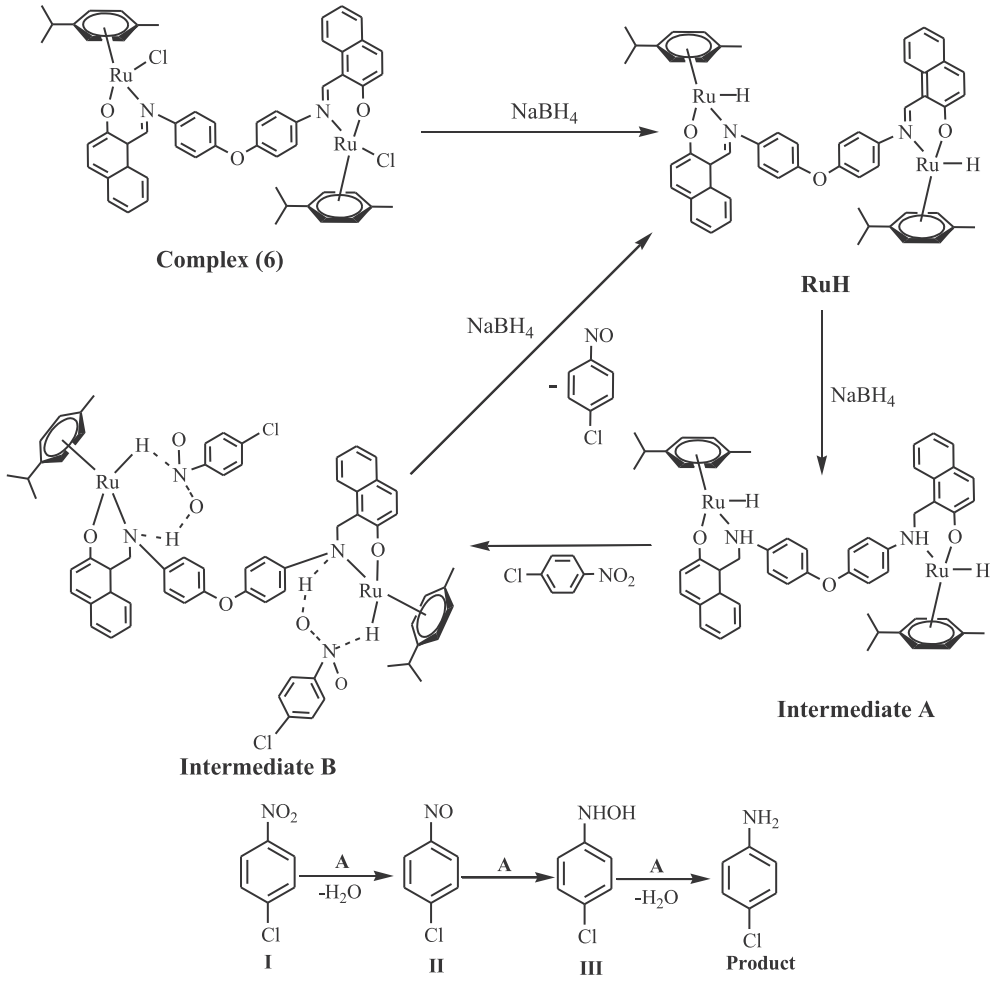


**Scheme 2.** Probable Mechanism for Reduction of Nitroarenes Catalyzed by Half-Sandwich Binuclear Ruthenium Complexes.

### 4.4. X-ray structure determination

Diffraction data of **(6)** were collected on a Bruker AXS SMART APEX diffractometer, equipped with a CCD area detector using Mo Kα radiation (λ = 0.710 73 Å). All the data were collected at 298 K, and the structures were solved by direct methods and subsequently refined on F2 by using full-matrix least-squares techniques (SHELXL) [45], SADABS [46] absorption corrections were applied to the data, all non-hydrogen atoms were refined anisotropically, and hydrogen atoms were located at calculated positions. All calculations were performed using the Bruker Smart program.

### 4.5. Computational details

Computational chemistry tools like DFT methods are already used successfully for the complete characterization of challenging molecules [47a-47e]. In order to overcome the effect of solvation and disorder resulted in the crystal structure of the molecule **6**, DFT calculations were used as a support for the predicted molecular structure. DFT calculations were carried out using the software ORCA developed by Frank Neese and co-workers [48a]. All calculations were performed using the BP86 density functional [48b-48e] and def2-TZVP basis set [48f] included in the ORCA programme, which is free for academic use. Molecular structure from X-Ray diffraction method was taken as initial geometry for the DFT calculations. Self-Consistent Field (SCF) calculations were performed using the TIGHTSCF convergence criteria. The geometry optimization was carried out and the resulting geometries are confirmed as minima through the frequency calculations, which show no imaginary frequencies. The reactivity descriptors like, Chemical potential (μ), Hardness (η), Softness(S), Electrophilicity (ω), Ionization potential (IP) and Electron Affinity (EA) are also calculated to predict the stability of the complexes. Pictures of the optimized geometries and the frontier molecular orbitals are taken using the graphics programme ChemCraft [48 g].

## Declaration of competing interest

The authors declare that they have no known competing financial interests or personal relationships that could have appeared to influence the work reported in this paper.

## Acknowledgments

The authors express sincere thanks to Single Crystal X–ray Diffraction Facility, SAIF Guwahati University, for providing X–ray data collection.

## Appendix A. Supplementary data

Supplementary data to this article can be found online at https://doi.org/10.1016/j.jorganchem.2019.120984.

## References


[1] C.S. Hauser, C. Slugove, K. Mereiter, R. Schmid, K. Kirchner, L. Xiao, Weissensteiner, J. Chem. Soc., Dalton Trans. (2001) 2989.
[2] (a) C.S. Allardyce, P.J. Dyson, D.J. Ellis, S.L. Heath, Chem. Commun. (2001) 1396–1397;
(b) H. Chen, J.A. Parkinson, S. Parsons, R.A. Coxall, R.O. Gould, P.J. Sadler, J. Am. Chem. Soc. 124 (2002) 3064–3082;
(c) R.E. Aird, J. Cummings, A.A. Ritchie, M. Muir, R.E. Morris, H. Chen, P.J. Sadler, D.I. Jodrell, Br. J. Canc. 86 (2002) 1652–1657;
(d) R.E. Morris, R.E. Aird, S. Murdoch, H. Chen, J. Cummings, N.D. Hughes, S. Parsons, A. Parkin, G. Boyd, D.I. Jodrell, P.J. Sadler, J. Med. Chem. 44 (2001) 3616–3621.
[3] H. Li, Z.-J. Yao, D. Liu, G.-X. Jin, Coord. Chem. Rev. 139 (2015) 293–294.
[4] Y.-F. Han, G.-X. Jin, Chem. Soc. Rev. 43 (2014) 2799–2823.
[5] Y.-F. Han, H. Li, Y. Fei, Y.-J. Lin, W.-Z. Zhang, G.-X. Jin, Dalton Trans. 39 (2010) 7119–7124.
[6] G.L. Wang, Y.-J. Lin, H. Berke, G.-X. Jin, Inorg. Chem. 49 (2010) 2193–2201.
[7] W.-Z. Zhang, Y.-F. Han, Y.-J. Lin, G.-X. Jin, Dalton Trans. 39 (2009) 8426–8431.
[8] Y.-F. Han, H. Li, G.-X. Jin, Chem. Commun. 46 (2010) 6879–6890.
[9] P. Singh, A.K. Singh, Organometallics 29 (2010) 6433–6442.
[10] R.M. Lord, A.J. Hebden, C.M. Pask, I.R. Henderson, S.J. Allison, S.L. Shepherd, R.M. Phillips, P.C. McGowan, J. Med. Chem. 58 (2015) 4940–4953.
[11] M. Ito, S. Kitahara, Ikariya, J. Am. Chem. Soc. 127 (2005) 6172–6173.
[12] E. Rodríguez Arce, C. Sarniguet, T.S. Moraes, M. Vieites, A.I. Tomaz, A. Medeiros, M.A. Comini, J. Varela, H. Cerecetto, M. González, F. Marques, M.H. García, L. Otero, D. Gambino, J. Coord. Chem. 68 (2015) 2923–2937.
[13] M.J. Chow, C. Licona, D.Y.Q. Wong, G. Pastorin, C. Gaiddon, W.H. Ang, J. Med. Chem. 57 (2014) 6043–6059.
[14] (a) F.C. Pigge, J.J. Coniglio, Curr. Org. Chem. 5 (2001) 757–784;
(b) J.H.M.A. Rigby, Kondratenko, Top. Organomet. Chem. 7 (2004) 181–204;
(c) , in: J. Gimeno, V. Cadierno, P. Crochet, R.H. Crabtree, D.M.P. Mingos (Eds.), Comprehensive Organomet. Chem., III, vol. 6, Elsevier, Oxford, 2007, pp. 465–550;
(d) B. Therrien, Coord. Chem. Rev. 253 (2009) 493–519;
(e) L. Delaude, A. Demonceau, Dalton Trans. 41 (2012) 9257–9268;
(f) P. Kumar, R.K. Gupta, D.S. Pandey, Chem. Soc. Rev. 43 (2014) 707–733;
(g) B. Therrien, CrysEngComm 17 (2015) 484–491.
[15] (a) S.I. Kozhushkov, L. Ackermann, Chem. Sci. 4 (2013) 886–896;
(b) S. De Sarkar, W. Liu, S.I. Kozhushkov, L. Ackermann, Adv. Synth. Catal. 356 (2014) 1461–1479.
[16] (a) R. García-Álvarez, J. Francos, E. Tomás-Mendivil, P. Crochet, V. Cadierno, J. Organomet. Chem. 771 (2014) 93–104;
(b) P. Crochet, V. Cadierno, Top. Organomet. Chem. 48 (2014) 81–118.
[17] (a) A.L. Noffke, A. Habtemariam, A.M. Pizarro, P.J. Sadler, Chem. Commun. 48 (2012) 5219–5246;
(b) F. Foubelo, C. Nájera, M. Yus, Tetrahedron: Asymmetry 26 (2015) 769–790;
(c) D. Wang, D. Astruc, Chem. Rev. 115 (2015) 6621–6686.
[18] M.J. Vaidya, S.M. Kulkarni, R.V. Chaudhari, Org. Process Res. Dev. 7 (2003) 202–208.
[19] A.M. Tafesh, Weiguny, J. Chem. Rev. 96 (1996) 2035–2052.
[20] R.K. Rai, A. Mahata, S. Mukhopadhyay, S. Gupta, P.-Z. Li, K.T. Nguyen, Y. Zhao, B. Pathak, S.K. Singh, Inorg. Chem. 53 (2014) 2904–2909.
[21] J. Liu, J. Cui, F. Vilela, J. He, M. Zeller, A.D. Hunter, Z. Xu, Chem. Commun. 51 (2015) 12197–12200.
[22] W.-G. Jia, Y.-C. Dai, H.-N. Zhang, X. Lu, E.-H. Sheng, RSC Adv. 5 (2015) 29491–29496.
[23] Z. Zhao, H. Yang, Y. Li, X. Guo, Green Chem. 16 (2014) 1274–1281.
[24] X.-J. Yang, B. Chen, L.-Q. Zheng, L.-Z. Wu, C.-H. Tung, Green Chem. 16 (2014) 1082–1086.
[25] X. Liu, S. Ye, H.–Q. Li, Y.-M. Liu, Y. Cao, K.-N. Fan, Catal. Sci. Technol. 3 (2013) 3200–3206.
[26] R.G. De Noronha, C.C. Romão, A.C. Fernandes, J. Org. Chem. 74 (2009) 6960–6964.
[27] A.B.P. Lever, Inorganic Electronic Spectroscopy, second ed., Elsevier, New York, 1984.
[28] K. Ghosh, R. Kumar, K. Kumar, A. Ratnam, U.P. Singh, RSC Adv. 4 (2014) 43599–43605.
[29] T.D. Thangadurai, K. Natarajan, Trans. Met. Chem. 25 (2000) 347–351.
[30] J. Dutta, M.G. Richmond, S. Bhattacharya, Eur. J. Inorg. Chem. (2014) 4600–4610.
[31] T.-T. Thai, B. Therrien, G. Süss-Fink, Inorg. Chem. Commun. 12 (2009) 806–807.
[32] R. Payne, P. Govender, B. Therrien, C.M. Clavel, P.J. Dyson, G.S. Smith, J. Organomet. Chem. 729 (2013) 20–27.
[33] P. Govindaswamy, B. Therrien, G. Süss-Fink, P. Stěpnicka, J. Ludvík, J. Organomet. Chem. 692 (2007) 1661–1671.
[34] R. Pettinari, F. Marchetti, C. Pettinari, A. Petrini, R. Scopelliti, C.M. Clavel, P.J. Dyson, Inorg. Chem. 53 (2014) 13105–13111.
[35] R.M. Lord, A.J. Hebden, C.M. Pask, I.R. Henderson, S.J. Allison, S.L. Shepherd, R.M. Phillips, P.C. McGowan, J. Med. Chem. 58 (2015) 4940–4953.
[36] J.G. Malecki, R. Kruszynski, M. Jaworska, P. Lodowski, Z. Mazurak, J. Organomet. Chem. 693 (2008) 1096–1108.
[37] R. Pettinari, C. Pettinari, F. Marchetti, C.M. Clavel, R. Scopelliti, P.J. Dyson, Organometallics 32 (2013) 309–316.
[38] J.G. Malecki, Struct. Chem. 23 (2012) 461–472.
[39] D. Zuccaccia, G. Bellachioma, G. Cardaci, C. Zuccaccia, A. Macchioni, Dalton Trans. (2006) 1963–1971.
[40] (a) A. Habtemariam, M. Melchart, R. Fernandez, S. Parsons, I.D. Oswald, A. Parkin, F.P. Fabbiani, J.E. Davidson, A. Dawson, R.E. Aird, D.I. Jodrell, P.J. Sadler, J. Med. Chem. 49 (2006) 6858–6868;
(b) Leli Zeng, Pranav Gupta, Yanglu Chen, Enju Wang, Liangnian Ji, Hui Chao, Zhe-Sheng Chen, Chem. Soc. Rev. 46 (2017) 5771–5804.
[41] A.K. Shil, P. Das, Green Chem. 15 (2013) 3421–3428.
[42] R. Nandhini, G. Venkatachalam, M. Deepan Kumar, M. Jaccob, Polyhedron 158 (2019) 183–192.
[43] M.A. Bennett, A.K. Smith, J. Chem. Soc. Dalton Trans. (1974) 233–240.
[44] W.-G. Jia, H. Zhang, T. Zhang, S. Ling Inorg, Chem. Commun. 66 (2016) 15.
[45] G.M. Sheldrick, Acta Crystallogr. A: Found. Crystallogr. 64 (2008) 112–122.
[46] G. Sheldrick, G. SADABS v, 2.01, Bruker/Siemens Area Detector Absorption Correction Program, Bruker AXS, Madison, WI, USA, 1998.
[47] (a) K. Bharathi, L. Beerma, C. Santhi, B.S. Krishnamoorthy, J.-F. Halet, J. Organomet. Chem. 792 (2015) 220–228, https://doi.org/10.1016/j.jorganchem.2015.05.057;
(b) B.S. Krishnamoorthy, S. Kahlal, S. Ghosh, J.-F. Halet, Theor. Chem. Acc. 132 (2013) 1356, https://doi.org/10.1007/s00214-013-1356-6;
(c) B.S. Krishnamoorthy, A. Thakur, K.K.V. Chakrahari, S.K. Bose, P. Hamon, T. Roisnel, S. Kahlal, S. Ghosh, J.-F. Halet, Inorg. Chem. 51 (2012) 10375, https://doi.org/10.1021/ic301571e;
(d) B.S. Krishnamoorthy, S. Kahlal, B. Le Guennic, J.-Y. Saillard, S. Ghosh, J.-F. Halet, Solid State Sci. 14 (2012) 1617, https://doi.org/10.1016/j.solidstatesciences.2012.03.026;
(e) K. Geetharani, B.S. Krishnamoorthy, S. Kahlal, S.M. Mobin, J.-F. Halet, S. Ghosh, Inorg. Chem. 51 (2012) 10176, https://doi.org/10.1021/ic300848f.
[48] (a) F. Neese, The ORCA program system, Wiley Interdiscip. Rev. Comput. Mol. Sci. 2 (2012) 73–78;
(b) S.H. Vosko, L. Wilk, M. Nusair, Can. J. Phys. 58 (1980) 1200–1211;
c) A.D. Becke, J. Chem. Phys. 84 (1986) 4524–4529;
d) A.D. Becke, Phys. Rev. A 38 (1986) 3098–3100;
(e) J.P. Perdew, Phys. Rev. B 33 (1986) 8822–8824;
(f) F. Weigend, R. Ahlrichs, Phys. Chem. Chem. Phys., 7 3297. (g) Chem craft, Graphical software for visualization of quantum chemistry computations. https://www.chemcraftprog.com.